Performance Analysis of a Cryogenic Induction Machine

Luís Fernando Dias Bucho,

Instituto Superior Técnico, University of Lisbon, Lisbon, Portugal

***Abstract*--Recent research, in the field of electric machines, has been focused on developing high power density designs to be used in new generation industrial and drive systems applications. These new developments have suggested the use of cryogenic induction motors as a reliable, efficient and low-cost solution, capable of outperforming the most advanced synchronous and reluctance motors.**

In this study the performance of a conventional 90W induction motor submerged in liquid nitrogen is analysed. The significant influence of both temperature and skin effect in the equivalent circuit parameters and the overall performance of the machine is analytically studied and experimentally proven. To validate the obtained analytical results, experimental procedures and experimental setups were developed using the induction machine submerged in liquid nitrogen.

The findings achieved in this work show that considerable improvements in torque and power densities can be made when operating an induction motor in very low temperatures.

The results show a 22.2\% increase in motor efficiency, from 63\% to 85.2\%. This significant increase in efficiency, results in a 170.8\% increase in torque and a 188.5\% increase in mechanical output power at peak efficiency.

***Index Terms*-- Cryogenic Induction Motor, Cryogenic Cooling, Electrical Machines, Electromechanical Performance, Liquid Nitrogen, Steinmetz Equivalent Circuit**

I. Introduction

The strive for maximum efficiency and maximum specific power in electric machines have been one of the main focus of the academy and industry since the first commercial electric motors were developed by Ferraris (G.Ferraris, 1888), Tesla (N.Tesla, 1888) and Dolivo-Dobrovolsky (Dolivo-Dobrovolsky, 1917)in the late 1880's, early 1890's. Since then, a number of improvements and different topologies were introduced to achieve the final goal of a reliable, more efficient, low cost and easy to control electric motor.

Both NEMA and the EU have, in the past 20 years put forward regulation, raising the efficiency requirements for new electric motors production (Council of European Union, 2019).This effort has had the intended result of increasing efficiency related research and create new, more efficient, manufacturing processes.

From the point of view of the induction motor, although these regulations and research have increased the efficiency of machines, it also highlighted some limitations present in this solid yet old design.

In the past, cryogenic cooling was something reserved for a few areas of interest in science, mainly in chemistry and physics research. This was true until the second world war. In the mid 1950's the technological race created a space where applied cryogenics would flourish, especially in manufacturing industry and military applications.

Today a few important applications, granted in very niche segments of industry and science, of cryogenic induction motors must be noted.

In the aerospace industry these cryogenic motors are commonly used as pumps to auxiliary fuel or cooling systems, mainly using liquid hydrogen (Redmond & Bott, 1964) working at a temperature of -253ºC. These cryogenic pumps are also used in advanced experimental physics research as in CERN (Claudet, 2017) and Nuclear research (Fast, 1992).

Furthermore, military applications such as ship and plane propulsion are also studied and implemented, coupled with superconducting machines (Tomsic, 2021).

The most common application in industry though is in the energy sector, cryogenic induction motors working as pumps in liquid gas transportation (Ai, Huang, & Wang, 2020).

All of these new improvements and applications allow one to think of cryogenic induction motors not as solely a requirement to superconducting machines but also an opportunity to improve efficiency of the current machines, either by especially designing cryogenic induction motors or even converting the existing convectional ones into cryogenic machines and improve significantly the efficiency and power density of these types of motors.

II. Electromechanical Modelling of Cryogenic Induction Machines

In this chapter the effect of cryogenic conditions on the performance of induction machines will be discussed. The steady-state equivalent circuit model of the induction machine is used to evaluate the effect of the temperature and skin effect, under cryogenic conditions, Figure 1. Lastly, results are obtained based on this model for the torque and efficiency characteristics.

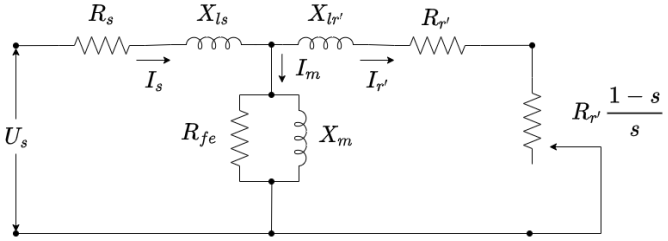

Figure 1. Induction machine equivalent circuit.

A. Influence of Cryogenic Temperature

Starting with influence of temperature on the equivalent circuit model's parameters, this analysis will go through the physical quantities that play a role in this influence and explain to what extent this influence occurs.

Most physical properties of a material or a system are influenced by temperature, from chemical reactions to macro thermodynamic processes. This influence in an electric machine is mainly due to the variation of electrical conductivity of the materials used to build the machine.

1) Stator Resistance, R_s

The parameter stator resistance R_s models the physically measurable DC resistance of the stator conductors made out of copper. This resistance is a function of the material resistivity ρ, its length l and A, the cross-sectional area of the conductor and is given by:

$$R = \rho \frac{l}{A} \tag{1}$$

While it is true that any of these physical quantities are influenced by temperature to some extent, the influence in the conductor length and cross-sectional area, due to contraction, is very small compared with the influence of temperature in the material resistivity, thus is usually neglected.

The estimation of a material resistivity as a function of temperature is usually done using the well-known one term linear equation (2).

$$\rho = \rho_0(1 + \alpha_{Cu}(T - T_0)) \tag{2}$$

where ρ is the material's resistivity at a given temperature, T, ρ_0 is the resistivity at the reference temperature, T_0, and α_{cu} is the material's temperature coefficient.

Assuming a copper temperature coefficient α_{cu} = 0.00386 (Giancoli, 1995) for the reference temperature of 20°C (293.15K) and considering that for 20ºC the resistivity of copper is $\rho_0 = 1.68 \times 10^{-8}$ Ωm:

$$\rho(T = -196ºC) = 2.7928 \times 10^{-9}\Omega m \tag{3}$$

Meaning that the resistivity of copper (ρ_{cu}) at 77K is 6.01 times lower than for 293.15K or 20ºC.

2) Rotor Resistance, R'_r

The parameter R'_r models the resistance of the rotor cage as seen from stator. Since the rotor cage is made out of aluminium, one can say that in a similar manner to the stator resistance, it too is affected by temperature. One may think that the analysis of the change in resistivity with respect to temperature for the case of aluminium follows the same procedure as done for the stator copper windings, but in fact it does not. This is because, when it comes to aluminium, the relation between resistivity and temperature for temperatures lower than 100K is non linear, meaning that equation (2) cannot be used.

Nonetheless this analysis is possible by making use of empirical data (Hucek, Wilkes, Hanby, & Thompson, 1977). Using the empirical data, it is possible to estimate the aluminium resistivity for the range of temperatures of interest in this thesis, by fitting a third-degree polynomial function:

$$\rho(T) = 7.742 \times 10^{-15}T^3 - 5.025 \times 10^{-13}T^2 + 2.99 \times 10^{-11}\mathrm{T} + 5.793 \times 10^{-9}\Omega m \tag{4}$$
$$50K \leq T \leq 100K$$

Resulting $\rho_{77K} = 8.66 \times 10^{-9}\Omega$m, a reduction of 4.03 related to the ambient temperature.

3) Equivalent iron losses resistance, R_{Fe}

The equivalent iron losses resistance R_{Fe} models the iron core losses in the induction machine. The iron core in these electrical machines can be made out of a wide range of silicon-steel. The use of different types of silicon steel means that the result of the analysis of the influence of temperature in the iron core greatly varies. Despite this, the average influence across the most common used grades of silicon steel is usually considered in the literature when an estimation of the effect is needed (Lv, Sun, & Sun, 2019).

From the literature it is know that the effect of temperature in the iron core is due, for the most part, to the increase of conductivity of the silicon steel σ and to a smaller extent the magnetic flux density B. From Bertotti classical loss separation model (Bertotti, 1988) it is know that the losses in the iron core P_{Fe} can be separated into two distinct groups, the hysteresis losses P_h and eddy current losses P_e.

From previous experiments (Lv, Sun, & Sun, 2019) hysteresis losses P_h are said to be constant with respect to temperature when the iron core is not saturated, this is the case for the machine tested in this thesis.

When it comes to eddy current losses, P_e, experimental data shows that these losses are directly proportional to the silicon-steel conductivity, and so an estimation of the impact of temperature in these losses must include an estimation of the increase in silicon steel conductivity at cryogenic temperatures. Usually for room temperature operation, a linear relation between conductivity and temperature is used to estimate the change in conductivity with respect to temperature, but this relation is not valid in cryogenic temperatures, where non-linear effects are present. Therefore, empirical data must be used to estimate this effect. According to (Lv, Sun, & Sun, 2019) the average increase of conductivity for the most common silicon steel at 77K compared to ambient temperature of 20ºC(295K) is [10-20]% and as such the equivalent iron losses resistance R_{Fe} should also decrease by around [10-20]%.

4) Stator and Rotor reactance, X_{ls} and X'_{lr}

This parameter models the magnetic energy that does not contribute to the main linked flux between the stator and the rotor. These leakage fluxes are mostly due to the geometry of the stator magnetic circuit and the windings connection arrangement. Because of this and as shown experimentally (Biasion, et al., 2021) it is usually considered that since the

effect of temperature on the machine geometry is negligible, and so is the effect of temperature in the stator and rotor's leakage reactance X_{ls} and X'_{lr}, meaning no change in this parameter should be observed.

5) Magnetizing reactance, X_m

Magnetizing reactance X_m models the magnetic energy present in the airgap of the induction machine which is the result of the linked magnetic flux between the stator and rotor. From the previous leakage reactances temperature influence analysis it was shown that magnetic properties of the machine's materials are not influenced by temperature, this is also true for this parameter which is therefore assumed constant.

B. Influence of Skin Effect

The skin effect is an electrodynamic phenomenon where the distribution of current in a conductor cross section is non uniform. This non uniform distribution of current, reduces the cross sectional, current carrying, area within the conductor, effectively reducing the conductor's cross-sectional area and hence increasing its resistance. Furthermore, the decrease of the effective conductor cross-sectional area also acts to decrease the conductor inductance.

This section concerns the analysis of the skin effect on the equivalent circuit parameters. Here it is going to be shown that the skin effect can have a significant impact on some parts of the machine and negligible on others, both negative and positive, which alters the performance of the machine and thus its equivalent circuit parameters. Furthermore, it is not possible to characterize the influence of the skin effect without including the effect that temperature has on conductivity, for which the skin effect is strongly dependent.

To aid in the analysis of the skin effect influence, one should start by introducing the concept of skin depth δ. The skin depth δ is defined as the depth below the conductor surface at which the current density falls to 1/e of the surface current density, and is given by equation (5), in the quasi-static regime.

$$\delta = \sqrt{\frac{2\rho}{\omega\mu}} \tag{5}$$

The skin effect is not visible on the stator resistance and leakage reactance, as the stator windings are made of multiple small diameters conductors (radius is much lower than the skin penetration).

1) Equivalent iron losses, R_{Fe}, and magnetizing reactance, X_m

The iron core of the machine is also made out of dozens of conductors isolated from each other, in the form of silicon-iron lamination's with a thickness of up to 1.5mm. Despite this fact, the electric and magnetic properties of the core silicon-iron alloy is very different from those of copper, mainly the magnetic permeability that is, at 20ºC, μ = 1.25×10^{-6} H/m for copper and μ = 5×10^{-3} H/m for FeSi, meaning almost 4000 times larger for the case of FeSi. Considering this, the skin depth values for the ambient and cryogenic temperatures are shown in (6) and (7), respectively.

$$\delta = 7.7522\times10^{-4}m = 0.7752\,mm \tag{6}$$

$$\delta = 1.9371\times10^{-4}m = 0.19371\,mm \tag{7}$$

Since the iron core lamination's thickness is around 0.5mm it is expected that under ambient temperature operation the skin effect influence is small but can be significant for machines with a lamination thickness of around 1mm. For the cryogenic case, this influence is expected to be important and cannot be neglected. This influence is going to be explored and validated trough experimental tests as this effect is usually neglected and an analytical model is not available.

2) Rotor resistance, R'_r, and rotor leakage reactance, X'_{lr}

In squirrel cage induction motors the rotor circuit is rather different from the stator one, the main difference being that contrary to the stator slots, rotor slots are fully filled by a solid conductors called the rotor bars.

As a first estimation of the influence of the skin effect in the rotor bars one should compute the skin depth. At 20ºC the aluminium resistivity is ρ_{Al} = 3.49×10^{-8} Ωm and the magnetic permeability is μ = 1.25×10^{-6} H/m. Therefore, the skin effect depth for the ambient and cryogenic conditions are shown in (8) and (9), respectively.

$$\delta = 0.0133m = 13.3\,mm \tag{8}$$

$$\delta = 0.0066m = 6.6\,mm \tag{9}$$

Since the height of the conductor is in the order of 1cm for this machine, it is apparent that the skin effect influence is important, especially in the cryogenic regime of operation.

The quantification of the skin effect influence in the equivalent circuit parameters is done by computing two coefficients, the resistance correction coefficient K_R, defined as the ratio between the AC and DC resistance of a conductor and the inductance correction coefficient K_L, defined as the ratio between the AC and DC inductance of a conductor.

The method used in this thesis is known as the multilayer approach method and was introduced in (Emde, 1922). The multilayer approach method consists of dividing the rotor bar into n layers with height h_p=h_t/n, width b_p and length l_{stack} as shown in figure 2.

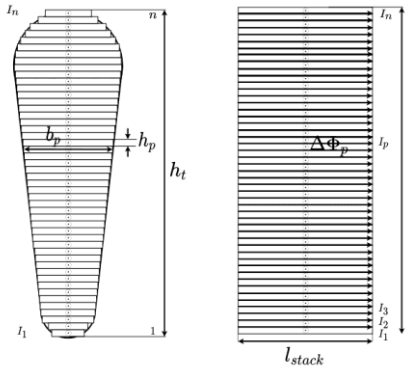

Figure 2. Division of solid conductors into layers

Applying Faradays Law to the p[th] layer, yields

$$R_p I_p - R_{p+1} I_{p+1} = -js\omega\Delta\phi_p \tag{10}$$

The current distribution in each layer of the slot can be obtained using:

$$I_{p+1} = \frac{R_p}{R_{p+1}} I_p + j\frac{s\omega L_p}{R_{p+1}} \sum_{n=1}^{p} I_n \tag{11}$$

Finally, the skin effect resistance and induction coefficient correction coefficients, K_R and K_L, can be computed using

$$K_R = \frac{P_{AC}}{P_{DC}} = \frac{\sum_{p=1}^{n} |I_p|^2 R_p}{\sum_{p=1}^{n} I_{pDC}^2 R_p} \tag{12}$$

$$K_L = \frac{W_{mAC}}{W_{mDC}} = \frac{\sum_{p=1}^{n} L_p \left|\sum_{k=1}^{p} I_k\right|^2}{\sum_{p=1}^{n} L_p \left|\sum_{k=1}^{p} I_{kDC}\right|^2} \tag{13}$$

where R_p and L_p are the resistance and induction coefficient of each layer of the slot. For ambient conditions these coefficients are K_R=1.0058 and K_L=0.9986 and for cryogenic conditions are K_R=1.0545 and K_L=0.9867.

C. *Numerical results*

In this section numerical results are to be presented. Torque and efficiency curves are to be simulated using the experimentally obtained equivalent circuit parameters analysed later in chapter IV. These numerical results are intended to give an estimation of the influence that both temperature and skin effect have in the performance of the machine as a whole.

1) Temperature influence

Figures 3 and 4 show the simulated torque and efficiency characteristic curves, respectively. In black, the simulated results for ambient temperature operation, in red, the simulated results for cryogenic operation assuming the whole machine is at 77K and, in blue, the simulated results for cryogenic operation assuming a rotor temperature of 97K and the rest of the machine at 77K.

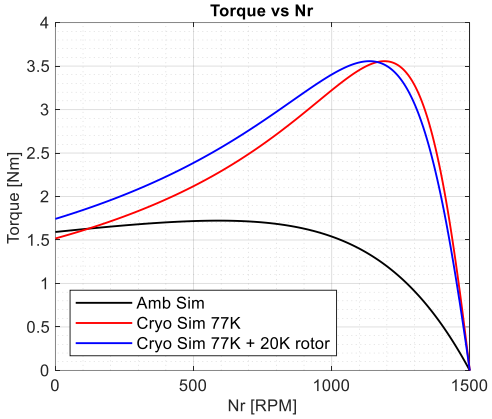

Figure 3. Torque temperature influence.

From figure 3 and looking at the black and red curves it is apparent that temperature has a very significant impact in the torque production throughout the whole range of slip.

First, the most obvious difference is the maximum torque. For ambient temperature peak torque is around 1.72Nm, at a rotor speed of 585RPM while in cryogenic temperature peak torque is around 3.56Nm at a rotor speed of 1191RPM. Meaning that peak torque is 2.07 times bigger in the cryogenic regime than in ambient temperature (relative difference of 106.98 %).

As observed in the simulations the starting torque of the machine in 77K is lower than the one in ambient temperature operation, with an expected starting torque of 1.59Nm for ambient operation and 1.52Nm for cryogenic operation, meaning a decrease of 4.40% in the starting torque.

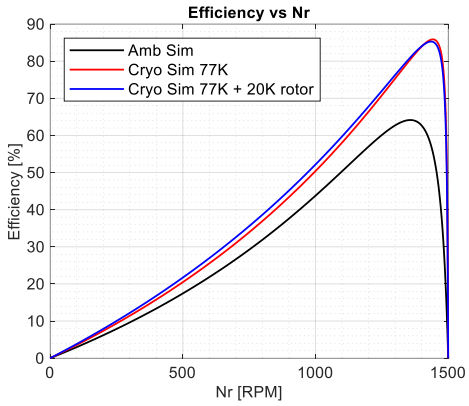

Figure 4. Efficiency temperature influence.

Regarding efficiency, from figure 4 it's expected that the maximum, for ambient temperature operation, is η = 64.15% at a rotor speed of N_r = 1358 RPM while for cryogenic operation η = 85.9% is expected, at a rotor speed of N_r = 1443RPM. An absolute increase of 21.75% is, therefore, expected. This significant increase is mainly due to the decrease in the stator losses, which dominate the losses in these very low power induction machines.

2) Skin effect influence

Figures 5 and 6 show, respectively, the simulated torque and efficiency characteristic curves for cryogenic operation. In black, the simulated results assuming no skin effect present, in

red, the simulated results with skin effect assuming the whole machine is at 77K, in blue, the simulated results assuming a rotor temperature of 97K and the rest of the machine at 77K with no skin effect included and in green, the same assumption as in the blue curve except this time with skin effect included.

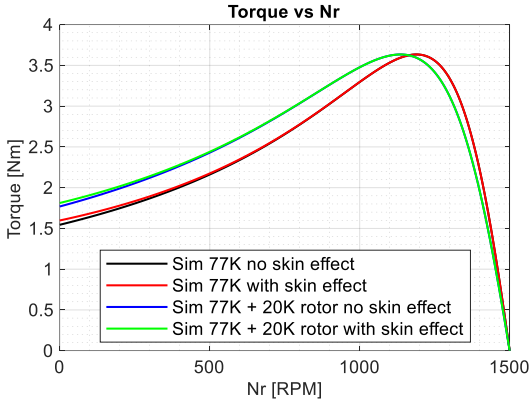

Figure 5. Torque skin effect influence.

From figure 5 its apparent that the increase of the rotor resistance R_r' (due to skin effect) causes an increase of start up torque as expected.

Observing the start up torque of the black curve compared to the red one, there is an increase of 3.49 % in the start up torque due to skin effect(1.55Nm to 1.6Nm). This increase is 2.25% when the rotor is at 97K, a smaller increase compared to the case where the whole machine is at 77K due to the increase of resistivity of aluminium.

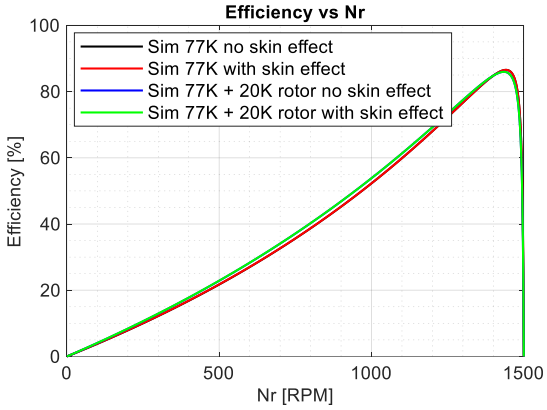

Figure 6. Efficiency skin effect influence.

Regarding efficiency it clear from figure 6 that the skin effect influence is negligible.

III. Experimental Setups and Methodology

Due to the presence of a cryogenic vessel, it was considered to use a vertical experimental setup with the induction machine immersed in LN_2, to avoid the use of sealant bearings. Two experimental setups were developed, one limited to 240W and other limited to 1000W.

A. Experimental setup 1

To test the induction machine under different loads, a DC machine is used. In this set-up a 240W 24V DC machine was used, with the characteristics listed in Table *1*. The built experimental setup 1 is shown in figure 7.

Table 1 – Nominal values of the 240W DC machine (load)

DC Machine nominal values	Armature circuit
Voltage	24 V
Current	10 A
Power	240 W
Speed	2000 RPM
Torque	1.15 Nm

Figure 7. Experimental setup 1.

Regarding the cryo-vessel, it was decided to build the LN_2 container using purely a polystyrene box (for the sake of speed and cost), however there was some difficulty in sealing it properly. The best way found to seal the LN_2 container was using thin strips of polystyrene, edged between the container body and the lid as well as using a thick double-sided tape for a better seal, while maintaining some leakage to avoid increase of pressure.

B. Experimental setup 2

This second experimental setup is introduced by the need to test the induction motor with higher loads. A 1kW 1500 rpm DC machine was used, with the characteristics listed in Table *2*. This new generator allowed for testing the induction machine under up to 1000W loads, five times bigger than the previous DC generator. As this machine is much heavier than the previous one, there was a need to build a new structure that would couple to setup 1 and allow the machine to be in the vertical position. This new structure is shown in figure 8.

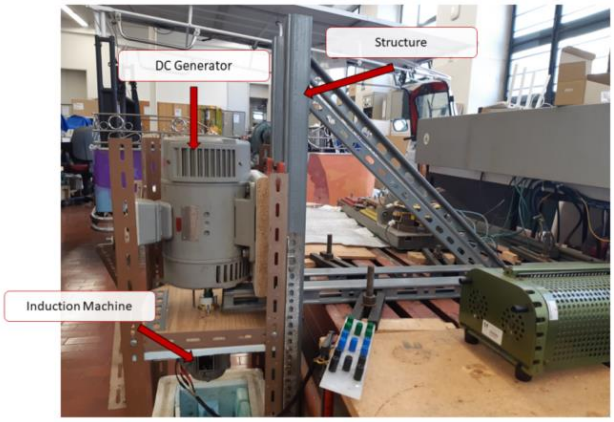

Figure 8. Experimental setup 2.

Table 2 – Nominal values of the 1kW DC machine (load)

DC Machine nominal values	Armature circuit	Field Circuit
Voltage	230 V	220 V
Current	4.4 A	0.55A
Power	1000 W	
Speed	1500 RPM	
Torque	6.37 Nm	

C. Bearings preparation

For this study, the choice of the type of bearings and grease are not only important but also crucial. This is, as expected, due to the very low temperatures that the machine is to be tested under. Most lubricants used today can handle a very wide spectrum of temperatures, usually from -50ºC up to 200ºC (SKF, 2021) or even higher temperatures. The same can be said for the types of materials and geometries of the bearings themselves. Since this motor is to be run at around -196ºC (77K), this choice must be carefully made, and have in consideration, the cost, availability, thermal amplitude sensitivity, no load and load friction coefficients.

The Induction motor studied in this thesis is a custom motor from Lafert, with standard bearings of the deep groove ball bearing type, made by SKF and built from stainless steel, with model number 6201-2Z. With no modifications whatsoever to the bearing, it quickly freezes in the liquid nitrogen bath.

Therefore, the grease from the bearings had to be removed, using an acetone bath. The solution is to let the bearing inside the acetone bath for about 5 days to a week, this was the time it required to completely clean out every residue of grease. It is important to add that every day the acetone should be changed, and that throughout these 5 to 7 days the bearing was tested many times, as previously explained, until it was possible to rotate it freely with no apparent formation of ice crystals. Figure 9 shows this process in action.

Figure 9. Grease removal process from the bearings.

D. Motor parameters experimental determination

To experimentally characterize the induction machine operating in cryogenic condition different experimental tests will be conducted: No-load, Blocked Rotor Tests and Load tests. From these, the influence of the temperature and the skin effect on the induction machine can be validated. In addition, load tests are also carried to analyse the improve of performance of the machine when operated in cryogenic conditions.

1) No-load Tests

The No-Load Test consists of testing the motor in a no-load condition, meaning that the load is removed from the setup and the rotor is to spin freely. Under this condition the rotor current is mainly the excitation current needed to create the rotating magnetic field.

At no-load, the active power consumed by the machine is given by the copper and iron losses, plus the mechanical ones.

$$P_{noload} = P_{Cu} + P_{Fe} + P_{mec} \tag{14}$$

Considering the equivalent circuit, and knowing the value of the stator's resistance, it is possible to compute not only the mechanical and iron losses, but also the equivalent iron losses resistance R_{Fe}

$$P_{noload} - 3R_s I_{sRMS}^2 - P_{mec} = \frac{3U_{mRMS}^2}{R_{Fe}} \tag{15}$$

The same can be done for the reactive power, allowing the estimation of the magnetizing reactance as

$$X_m = \frac{3U_{mRMS}^2}{Q_{noload}} \tag{16}$$

As described by equation (15), the iron losses are proportional to the square of magnetizing voltage, U_m. This means that for small values of U_m, close to 0, core losses are negligible, the mechanical losses can be computed. With the evolution of the no-load losses, the iron losses resistance and the mechanical losses can be computed, as shown in Fig. 10.

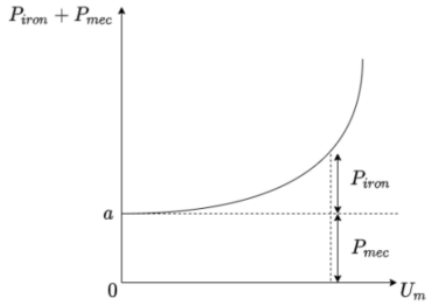

Figure 10. Separation of iron and mechanical losses.

2) Blocked Rotor Tests

The Blocked Rotor Test consists of testing the motor under rated current with its rotor mechanically blocked, to guarantee that the rotor is stationary. This test, analogous to a transformer short circuit test, gives information about stator and rotor leakage reactances and resistances.

In this test, both reactive and active power magnitudes are proportional to the square of the stator current, as shown in (17) and (18)

$$P_{blockedrotor} = 3(R_s + R_r')I_{sRMS}^2 \tag{17}$$

$$Q_{blockedrotor} = 3(X_{ls} + X_{lr}')I_{sRMS}^2 \tag{18}$$

Taken this into account, the power vs current curve can be modelled by quadratic functions and trough the fitting of the experimental results, the rotor and stator parameters can be estimated.

IV. Results

In this section, the experimental tests performed to the induction machine in both room temperature and cryogenic conditions are detailed. From the experimental results, the methodology presented in the modelling chapter is validated. First, the room temperature tests are performed to obtain the equivalent circuit parameters at normal conditions, and then, the cryogenic tests are performed to validate the change of these parameters with the cryogenic temperature.

Before performing the ambient temperature tests, the fan that was incorporated to the shaft of the induction machine was removed. This was done because the fan was made of plastic that would break under cryogenic temperatures, besides introducing turbulence in the liquid nitrogen.

A. Ambient temperature tests

In this section Ambient temperature tests results are analysed. The No-Load, Blocked Rotor and Load tests are compared with the simulated torque and efficiency curves, obtained from the parameters extracted using the previous tests. The results obtained in these tests will act as the baseline case, from which the later experimental results are to be compared.

1) No-load Test

Following the test procedure previously detailed, the first ambient temperature tests were performed. In figure 11 are shown, in dots, the experimental points obtained for the iron and mechanical losses and the reactive power, as a function of the machine magnetizing voltage, and in a continuous line the interpolation. An important detail is that, for these tests, the bearings were run in their original state, meaning, still with the manufactures grease, providing lubrication.

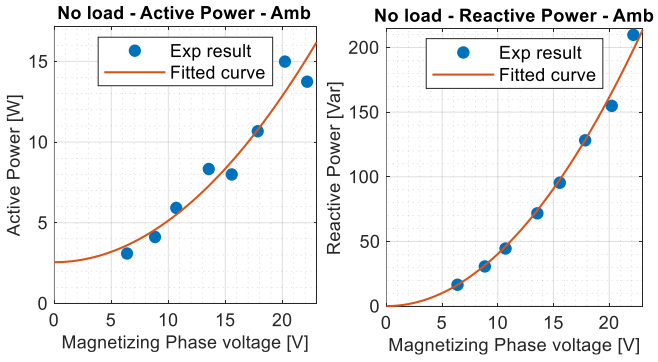

(a) Active power curve (b) Reactive power curve

Figure 11. Active and reactive power at no-load, under ambient temperature.

The decoupling of copper losses P_{Cu} from the total active power consumed by the machine is possible since the actual stator resistance and current were experimentally measured and thus copper power losses were computed. Also, and as seen before a quadratic function (in red) with a DC offset is fitted to these measured points. From this curve, mechanical power loss P_{mec} and equivalent iron losses resistance R_{Fe} is computed. As expected, for low values of magnetizing voltage $U_m < 5V$ (and thus stator voltage) the active power consumed by the machine (again, excluding copper losses) is fairly constant and is about 2.55W. It is now possible to compute the equivalent iron losses resistance R_{Fe}, given by the constant coefficient of this quadratic relation (active power as a function of the square of magnetizing voltage) which leaves us with $R_{iron} = 116.4\Omega$.

In a similar manner to the previous case, the reactive power curve is analysed. In Table *3* the results are summarized.

Table 3 – Summarized results from the No-load Tests

No-load Tests – Amb. Temp	
Parameter	
R_{Fe}	116.4 Ω
X_m	7.33 Ω
Power losses (peak)	
P_{mec}	2.55 W
P_{Fe}	12.7 W

2) Blocked rotor test

The blocked rotor tests were performed under normal operating grid frequency of 50Hz. Also, the input voltage is reduced significantly as to impose the nominal current of 3.66A. In figure 12 a), experimental active power magnitude data is plotted against the quadratics fitted curve in red. The results show that for a stator current average magnitude across the three phases of 3.55A close to the nominal one (I_S = 3.66 A), the active power consumed by the machine is 81W. Since the rotor is blocked, and no work is being done, this value of active power consumptions is due to Joule losses in the stator copper windings as well as Joule losses in the rotor caused by the induced currents flowing across the short-circuited aluminium cage.

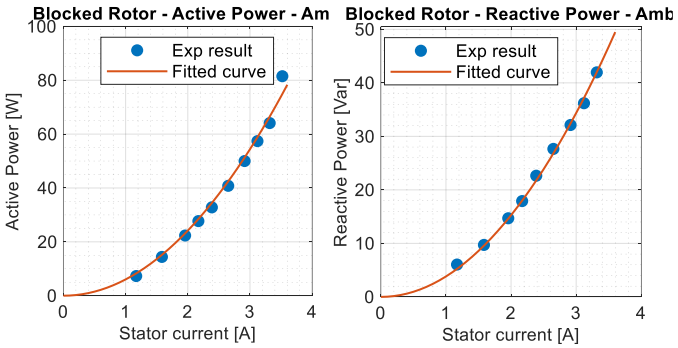

(a) Active power curve (b) Reactive power curve

Figure 12. Active and reactive power at rotor blocked tests, under ambient temperature.

From figure 12 (a) and since the stator windings resistance R_s can be directly measured, it's possible to compute the rotor resistance R_r' seen from stator, which results in R_r' = 0.914Ω.

From figure 12 b) data shows that under nominal stator current and with the rotor blocked there is a consumption of around 46 Var of reactive power. Contrary to the previous case where the stator resistance R_s can be physically measured, in this case it is extremely difficult to directly measure only the stator leakage inductance. The usual procedure is to consider that the value of leakage reactances of the stator and rotor is the same.

In Table 4 the results are summarized the results for the equivalent parameters obtained.

Table 4 – Summarized results from the blocked-rotor Tests

No-load Tests – Amb. Temp	
Parameter	
R_S	1.1 Ω
R'_R	0.914 Ω
X_S	0.532 Ω
X'_R	0.532 Ω

3) Load tests

After the No Load and Blocked Rotor tests, the computation of the induction machine performance is simulated using the experimentally obtained equivalent circuit parameters. In figure 13 are shown the simulated torque-speed and efficiency-speed curves, together with the experimental results for different loads (dotted points).

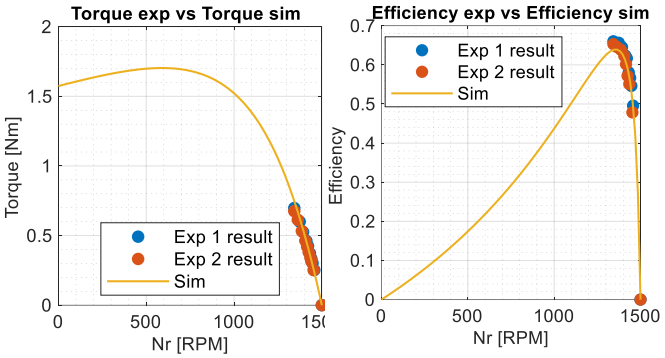

(a) Torque characteristic (b) Efficiency characteristic

Figure 13. Torque-speed and Efficiency-speed curves at ambient temperature tests.

Figure 13 a) and b) shows that the obtained experimental results follow the simulated curves as expected, although not perfectly. The obtained differences between the experimental data (dotted data) and the simulation, a 2.03% error, are the result of differences in temperature between the simulation and ambient temperature at the time of the tests and the constant regulation of the input voltage due to the internal voltage drop in the autotransformer. Nevertheless, the experimental results are close to the simulation ones, thus verifying the model and its parameters.

B. Cryogenic temperature tests

With the machines ambient temperature operation analysed, cryogenic tests are followed. As explained in chapter III the operation of the machine submerged in liquid nitrogen requires some preparation.

1) No-load Test

Cryogenic No-Load tests follow the same procedure as in Ambient temperature operation, with a few added difficulties. These difficulties were related to the cryogenic environment itself, which most have already been described in previous chapter III. In figure 14 are shown the active and reactive power at the no-load condition.

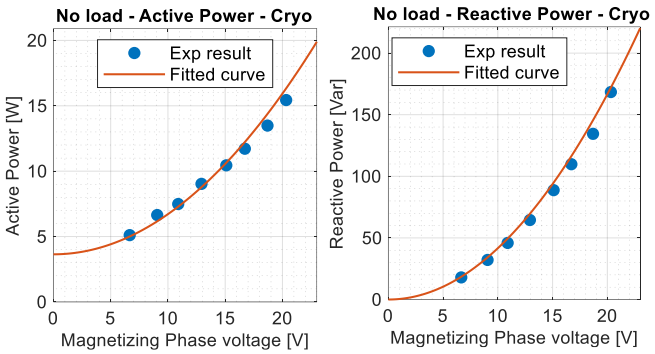

(a) Active power curve (b) Reactive power curve

Figure 14. Active and reactive power from the no-load tests at cryogenic temperature.

As observed, the results are coherent with the expected behaviour from this test, and correlation between the theoretical curve and the measurements is very good (R^2 = 0.985). The same analysis made for the ambient temperature case is done here. From the fitted curve the obtained maximum value of mechanical power losses is P_{mec} = 3.64W. Furthermore, maximum iron power losses value was also computed, with the value of P_{Fe} = 15.1W. With this, the equivalent iron losses resistance parameter computation follows, with a final result of R_{Fe} = 97.6Ω. Maximum reactive power consumed by the induction motor in this test was 222.86Var, at nominal stator voltage. Furthermore, from the analytical fitted curve magnetizing reactance was computed, the result is a value of X_m = 6.97Ω. In Table 5 the results are summarized.

Table 5 – Summarized results from the No-load Tests

No-load Tests – Cryo. Temp	
Parameter	
R_{iron}	97.6 Ω
X_{mag}	6.97 Ω
Power losses (peak)	
P_{mec}	3.64 W
P_{iron}	15.1 W

2) Blocked rotor Test

After the No Load Test, a series of Blocked Rotor tests were performed. These tests follow the same procedure as in the ambient temperature operation, and the same precautions highlighted for the cryogenic tests are followed here. The fact that heat can be extracted from the machine fairly quickly grants an opportunity of going beyond the nominal current in this test, this is not possible in ambient temperature operation, as the machine to air heat transfer flux is insufficient to maintain a temperature where the integrity of the machine's material is guaranteed. This opportunity might give an insight into some problems and effects that may happen to the machine in this environment, when currents go far beyond the nominal ones, as in motor start-up.

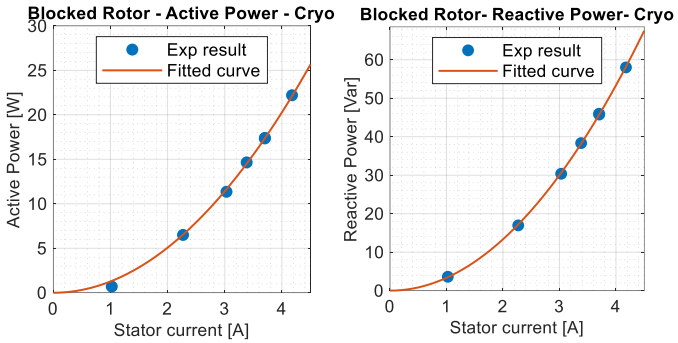

(a) Active power curve (b) Reactive power curve

Figure 15. Active and reactive power from the blocked rotor tests at cryogenic temperature.

As explained before, maximum stator current in this test is above the nominal current, with a value of 4.18A it is 14.21% above the nominal one. Despite this no unexpected behaviour is shown in the measured data, it is clear that even for these larger currents, the analytical curve fully models active power consumption. Maximum active power reached in this test is 22.20W, with this information and using the measured stator resistance at 77K (-196ºC), with a value of 0.2Ω, the obtained rotor resistance is computed to be $R_r^{'}$= 0.223Ω. In the same manner as previously noted, leakage reactance parameters were computed, the obtained stator and rotor leakage reactances are shown in the Table 6, summarizing all of the obtained results in the Blocked Rotor Tests.

Table 6 – Summarized results from the blocked-rotor Tests

No-load Tests – Cryo. Temp	
Parameter	
R_S	0.2 Ω
R'_R	0.223 Ω
X_S	0.556 Ω
X'_R	0.556 Ω

3) Load tests

Cryogenic tests were performed using both experimental setups described in section III, the first tests were performed using the first experimental setup for its easiness of assemble and use. Later tests were performed using the second experimental setup to be able to test the machine close to its maximum torque. Figure 16 shows Torque vs Speed and Efficiency vs Speed plots for the final results.

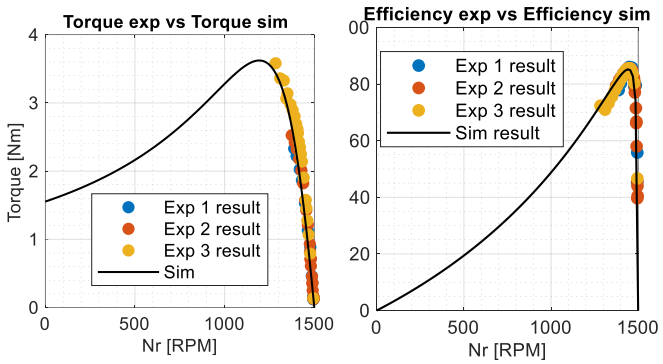

(a) Torque characteristic (b) Efficiency characteristic

Figure 16. Torque-speed and Efficiency-speed curves at cryogenic temperature.

The obtained results are aligned with the expected. The maximum stator current reached in these tests was short of 16A, at an average stator current of 15.14A across the three phases, a maximum of 3.58Nm of torque was reached. This was achieved at 72.4 % efficiency and at 1284RPM rotor speed. This maximum torque was not possible to reach though, despite a few attempts, this was due to, the expected, instability of this region of operation. Also, the previous maximum efficiency point was in this case also confirmed to be 85.5% at 1441RPM.

C. Comparison between ambient temperature and Cryogenic operation

In this section the obtained experimental results from ambient and cryogenic operation are discussed. First equivalent circuit parameters difference is analysed followed by torque and efficiency results, also difference in losses between both regimes are also going to be analysed as to fully characterize and summarize the findings in this thesis. Results for the equivalent circuit parameters are summarized in Table 7.

Table 7 – Summarized results from ambient and cryogenic operation

Parameter	Amb. Temp.	Cryo. Temp.	Difference
R_S	1.1 Ω	0.2 Ω	-81.8 %
$R_r^{'}$	0.914 Ω	0.223 Ω	-75.6 %
X_{ls}	0.532 Ω	0.556 Ω	+4.5%
$X_{lr}^{'}$	0.532 Ω	0.556 Ω	+4.5%
R_{Fe}	116.4 Ω	97.6 Ω	-16.1 %
X_m	7.33 Ω	6.97 Ω	-4.9 %

Regarding operational performance, the peak values for the torque, mechanical power, efficiency and losses are shown in Table 8. The most notorious result is the increase of efficiency from 63.9% to 85.2 % and the increase of rated torque from 0.72 Nm to 1.95 Nm when operating at cryogenic conditions.

Table 8 – Summarized performance for ambient and cryogenic operation

	Amb. Temp.	**Cryo. Temp.**	**Difference**
Maximum Efficiency	63.9 % (@s=10.9%)	85.2 % (@s=4%)	+33.3%
Torque ($@\eta_{max}$)	0.72 Nm	1.95 Nm	+170.8%
Mechanical Power ($@\eta_{max}$)	101.9 W	294.3W	+188.5 %
Mechanical losses	2.55 W	3.64 W	+42.8 %
Iron losses (peak)	12.7 W	15.1 W	+19.3 %
Stator copper losses (peak)	35.9 W	23.35 W	-35.0 %

Finally, the following figures show a comparison between the ambient temperature and cryogenic torque-speed and efficiency-speed curves. It can be clearly seen the improvement of the induction machine performance.

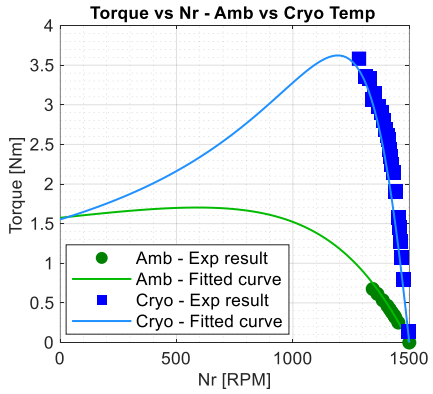

Figure 17. Torque-speed curves at ambient and cryogenic temperature.

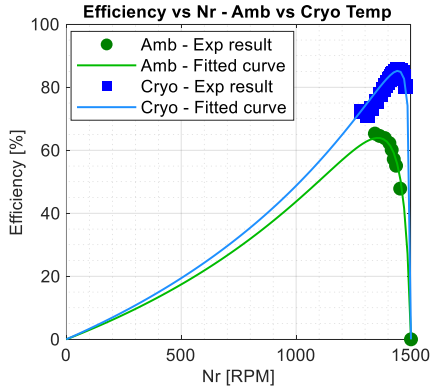

Figure 18. Efficiency-speed curves at ambient and cryogenic temperature

V. Conclusions

In this thesis the performance of a conventional air-cooled induction motor submerged in liquid nitrogen was analysed by comparing it to its ambient temperature performance.

Regarding the motor's overall performance and losses, the results indicate significant advantages in the motor operation in cryogenic temperatures. Despite a small increase of mechanical losses (1.1W), expected in liquid nitrogen operation, and, the confirmed, 19.3% increase in iron losses due to increase conductivity of the iron core, the significant 35% decrease in joule losses result in an absolute increase of 21.3% in efficiency, from 63.9% to 85.2%.

This efficiency improvement in the electromagnetic to mechanical power conversion, results in an increase of 170.8% in torque and 188.5% in mechanical power at peak efficiency, showing that significant improvements in power and torque densities can be made when operating an induction motor in very low temperatures.

VI. References

[1] G.Ferraris. (1888). Electrodynamic Rotation by means of Alternating Currents. *The Journal of the American Institute of Electrical Engineers*.

[2] N.Tesla. (1888). A New System of Alternate Current Motors and Transformers. *The Journal of the American Institute of Electrical Engineers*.

[3] Dolivo-Dobrovolsky, M. (1917). Aus der Geschichte des Drehstroms. *ETZ Elektrotechnische Zeitschrift*(26-29), 341-344,354-357,366-369,376-377

[4] Council of European Union. (2019, October). COMMISSION REGULATION (EU) 2019/1781. 74-94. Official Journal of the European Union.

[5] Redmond, J. H., & Bott, F. W. (1964). Development of Cryogenic Electric. *SAE Transactions, 72*.

[6] Claudet, S. (2017, June). Retrieved from Cryogenics, CERN: indico.cern.ch/event/565314/contributions/2285754/attachments/1472534/2279197/CAS_Sweden_Cryo_2017_sc.pdf

[7] Fast, R. (1992). Development of a large centrifugal cryogenic pump. In *Advances in Cryogenic Engineering* (Vol. 37, pp. 845-851). Plenum Press.

[8] Tomsic, M. (2021, January). Retrieved from Hyper Tech Research,ARPA-E: arpa-e.energy.gov/sites/default/files/2021-03/10_Hyper%20Tech%20ARPA-E%20ASCEND%20Slide%20Presentation-kickoff%20meeting%20Final_pdf.pdf

[9] Ai, C., Huang, Y., & Wang, H. (2020, December). Coupled Electromagnetic and Thermal Analysis of a 15kW Cryogenic Induction Motor for Submerged Liquefied Natural Gas Pumps. *IEEE*. doi:10.23919/ICEMS50442.2020.9290937

[10] Giancoli, D. C. (1995). *Physics* (1 ed.). Prentice Hal.

[11] Hucek, H. J., Wilkes, K. E., Hanby, K. R., & Thompson, J. K. (1977). *Handbook on Materials for Superconducting Machinery* (1 ed.). Metals and Ceramics Information Center.

[12] Lv, X., Sun, D., & Sun, L. (2019, December). Determination of Iron Loss Coefficients of Ferromagnetic Materials Used in Cryogenic Motors. *IEEE*. doi:10.1109/ICEMS.2019.8922160

[13] Bertotti, G. (1988, January). General properties of power losses in soft ferromagnetic materials. *IEEE Transactions on Magnetics*. doi:10.1109/20.43994

[14] Biasion, M., Fernandes, J. F., Branco, P. J., Vaschetto, S., Cavagnino, A., & Tenconi, A. (2021). A Comparison of Cryogenic-Cooled and Superconducting Electrical Machines. *IEEE*.

[15] Emde. (1922). About Current Redistribution. 301. EUM.

[16] SKF. (2021). *Technical specifications of SKF standard and special greases for capped deep groove ball bearings. Table 1.* Retrieved from /www.skf.com/group/products/rolling-bearings/engineered-products/hybrid-bearings/temperature-limits